RSC Advances

PAPER

View Article Online
View Journal | View Issue

Cite this: *RSC Adv.*, 2024, **14**, 3379

Ilmenite-derived titanic acid species: exploring their outstanding light-independent antibacterial activity

Nadeera Dilshan Wickramasinghe,[a] A. H. Janaka Sampath,[a] Chandrika M. Nanayakkara,[b] K. M. Nalin de Silva[a] and Rohini M. de Silva*[a]

The emergence of resistance in detrimental pathogenic bacteria towards well-recognized antibiotics has greatly impacted global medicine, consequently exploring potent antibacterial compounds is becoming a potential area of research. Although photocatalytic metal oxides have been extensively explored in this regard, their applicability is diminished due to the requirement of photon energy. Therefore, in our study, we explored the light-independent antibacterial effect of two unexplored titanium species, known as metatitanic acid (MTA) and potassium titanate, against *Staphylococcus aureus*, *Escherichia coli*, and *Pseudomonas* spp. using the disk diffusion method in Luria–Bertani agar medium, where the well-known antibiotic, gentamicin, was used as the positive control. These two titanium compounds were readily synthesized through a novel process which was originally developed for the extraction of TiO_2 from ilmenite. The synthesized MTA was characterized using FT-IR, Raman spectroscopy, XRD, TGA, UV-visible spectroscopy, and SEM. According to our findings, both MTA and potassium titanate exhibited superior light-independent antibacterial properties, where for some concentrations, the effect was even greater than gentamicin. However, nano-TiO_2 totally failed as an antibacterial compound against the tested three strains under dark conditions.

Received 24th October 2023
Accepted 5th January 2024

DOI: 10.1039/d3ra07262b

rsc.li/rsc-advances

1 Introduction

Antibacterial agents are widely used in hospital-based clinical applications to kill or prevent bacteria growth, a common source of hospital-acquired infections.[1] These chemicals can act destructively in constructing cell walls, DNA synthesis, and protein synthesis without harming human cells.[2,3] These antibiotics can be classified into three groups, namely beta-lactams, macrolides, and quinolones, according to their mode of action, such as blocking the cross-linking during cell wall construction, cessation of protein synthesis binding to 50S subunit preventing translation and arresting DNA synthesis interfering with DNA topoisomerase and gyrase which are involved in DNA replication, respectively.[3] However, due to the extensive use of these drugs in human and veterinary medicine and indiscriminate use, the number of drug-resistant bacteria is increasing, making infections more complicated to treat and increasing the severity of illnesses and associated motility.[4] What is more alarming is the emergence and spread of antimicrobial-resistant bacteria with new resistance mechanisms threatening the ability to treat even common infections. Hence, there is a growing demand for novel antimicrobials to nullify the drawbacks associated with conventional antibiotics[4] that lead to longer hospital stays, higher medical costs, and increased mortality.

For this purpose, inorganic nanoparticles such as titanium dioxide,[5–8] zinc oxide,[9–13] copper oxide,[14–16] and silver[17–19] have been widely studied as potential antibacterial compounds and most of them are currently used in clinics.[20,21] Of these materials, titanium species have obtained higher merits due to their excellent photocatalytic activity, leading to the formation of reactive oxygen species (ROS) such as hydroxyl, oxo, and peroxo in the presence of UV radiation exposure.[22,23] These high-energy species can attack the bacterium, negatively contributing to its vital processes and inhibiting growth.[24] Since it is essential to have an irradiation source like UV, there is a greater difficulty in applying this to large-scale clinical uses. Therefore, it would be beneficial and practical if materials exhibited light-independent antibacterial activity.

Titanic acid species are acidic substances having titanium, oxygen, and hydrogen. Although there is a wide variety of titanic acids, including poly acids with layered structures, metatitanic acid (MTA), which has scarcely been studied, is an isolated form with the chemical formula H_2TiO_3.[25–28] The antibacterial effect of MTA and other titanate species has not been heavily investigated.[29] Synthesis of MTA using conventional methods is associated with significant drawbacks, including higher time

[a]*Centre for Advanced Materials and Devices (CAMD), Department of Chemistry, University of Colombo, Colombo 00300, Sri Lanka. E-mail: rohini@chem.cmb.ac.lk; Fax: +94714406263*

[b]*Department of Plant Sciences, University of Colombo, Colombo 00300, Sri Lanka*

consumption, use of non-greener harsh conditions, and utilization of expensively prepared titanium dioxide.[27,28] We isolated MTA as an intermediate in our ongoing research to develop a cost-effective and greener process for TiO_2 from Pulmoddai ilmenite in Sri Lanka. Here, in this study, we offered to prepare MTA as a valuable intermediate in the synthesis process of TiO_2 from the Pulmoddai ilmenite in Sri Lanka (awaiting patent). We explored the capacity of MTA and its potassium salt in the quest for light-independent antibacterial materials.

This study investigated the light-independent antibacterial effect of MTA and potassium titanate against Gram-negative and Gram-positive bacterial species, namely, *Staphylococcus aureus*, *Escherichia coli*, and *Pseudomonas* spp. In addition to the light-independent activity, the light-dependent activity of the two compounds was also evaluated and compared with respect to three bacterial strains. Additionally, these titanium intermediates were compared with the antibacterial activity of nano-TiO_2 (nano-titania) under light and dark conditions.

2 Materials and methods

2.1. Chemical reagents

All the chemicals used in this study were of analytical grade. Nanotitania powder (purchased from Sigma Aldrich with 21 nm primary particle size proven with TEM and 99.5% purity), potassium hydroxide (>85%, purchased from Fluka), sodium chloride (>99%, purchased from Sigma Aldrich), barium chloride (>99%, purchased from Fluka), sulphuric acid (98%, purchased from Sigma Aldrich), agar, peptone, yeast extract (purchased from Genshin Biotech), Mueller–Hinton and Luria–Bertani (LB) agar were purchased from Himedia, gentamicin (80 mg/2 mL) and sterile saline water were purchased from a local pharmacy.

2.2. Preparation of MTA and potassium titanate

MTA was synthesized and purified using a novel process using ilmenite as the raw material. First, ilmenite was digested with an acidic salt at 240 °C for 4 hours. The digested product was hydrolyzed with distilled water. The filtrate of the hydrolyzed solution was aged for 1 h at 90 °C. The product was purified by washing with a diluted mineral acid to obtain purified solid MTA. Oven-dried MTA solid particles were then reacted with 2 M KOH to get the potassium titanate suspension.

2.3. Characterization of synthesized MTA

Morphological features of synthesized MTA were observed through SEM – ZEISS EVO 18 machine under the magnification 3000 at 10.00 kV. Structural characterization of MTA was carried out through the X-ray diffractometer (Rigaku, Smartlab with Cu Kα radiation, 0.02° step size, over the 2θ range of 2–80° at a scanning speed of 10° min^{-1}), FT-IR spectrometer (PerkinElmer spectrum 2, software version 10.5.2, within the range of 550–4000 cm^{-1} under the resolution of 4) and Raman spectrometer (with compact TEM00 mode solid state lasers for illuminations as using 532 nm with maximum 200 mW power output). UV visible spectrometer (Thermo Scientific™ GENESYS™ 10S) with a Dual Beam-Internal detector was used to record the absorption spectrum of MTA. The thermal stability of MTA was studied by Thermo Gravimetric Analysis (TGA-SDT Q600; the sample was heated up to 1000 °C with a heating rate of 10 °C per minute under normal atmospheric conditions).

2.4. Antibacterial assay

Antibacterial activities of MTA and potassium titanate were assessed against three bacterial species (*S. aureus*, *Pseudomonas* spp. and *E. coli*) by disc diffusion and well diffusion methods. The comparison studies were carried out with nano-titania as well. The pure cultures were obtained and sub-cultured in nutrient agar plates in order to get 24 hours of active cultures for the assay. Bacterial suspensions containing 1×10^8 CFU mL^{-1} were prepared in sterile 1% NaCl solution using 0.5 McFarland turbidity standard to indicate cell density. A volume of 100 μL of each bacterial suspension was spread on each LB agar plate separately and kept for 30 minutes to absorb liquid into the medium. From stock solutions of the three antimicrobial agents (MTA, potassium titanate, and nano-titania), nine working solutions were prepared for each antimicrobial agent in the concentration range from 100 mg L^{-1} to 500 mg L^{-1} with 50 mg L^{-1} intervals. Sterile paper disks with the same dimensions were saturated with respective antibacterial solutions and placed on LB plates together with negative and positive controls. Sterile paper disks loaded with sterile distilled water and a 400 mg L^{-1} gentamicin solution were used as negative and positive controls, respectively. Plates were incubated at room temperature for 24 hours in a dark environment and in the presence of visible light. Three replicates were maintained for each bacterium and concentration. After 24 hours, inhibition zone diameters of bacterial growth were measured in three diagonals. All tests were triplicated following the same protocol.

2.5. Statistical analysis

Data were analyzed using One Way ANOVA and multiple mean comparison tests using Minitab 16.1 statistical software.

3 Results and discussion

3.1. Characterization

3.1.1. FT-IR analysis of MTA. Fig. 1 depicts the FT-IR spectrum of synthesized MTA, where several prominent absorptions could be detected at vibrational frequencies such as 3400, 3017, 1682, 1387, 1308, 1004, and 865 cm^{-1}. The weak and broad absorption near 3400 cm^{-1} can be assigned to water molecules physisorbed on the surface of MTA particles. The moderately sharp peak at 3017 cm^{-1} can be sensibly credited to stretching vibrations of structural hydroxyl groups (–OH) of MTA, of which bending vibrations must have given rise to the strong peak at 1682 cm^{-1}.[30,31] The stretching vibrations of S=O bonds in free SO_4^{2-} groups, which might be endowed from H_2SO_4 during the synthesis or through the washing step, are revealed by multiple absorption peaks at 1387 and 1308 cm^{-1}.[32] Furthermore, the IR peak at 1004 cm^{-1} is related with the stretching vibrations of Ti=O, while the IR absorption at

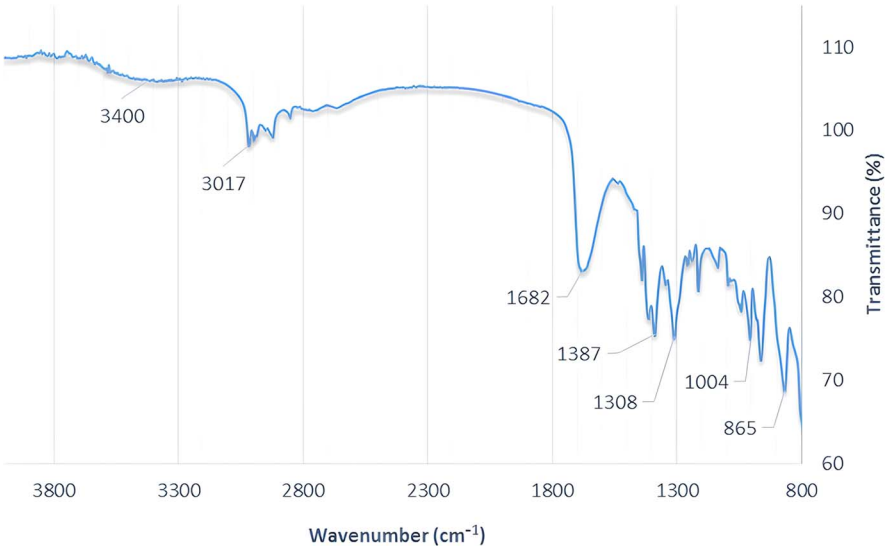

Fig. 1 The FT-IR spectrum of MTA.

865 cm^{-1} characterizes the bending vibrations of O–Ti–O moieties. As a whole, the structure of MTA can be judiciously proven due to the presence of IR absorption peaks corresponding to structural –OH, T=O, and O–Ti–O moieties.[33]

3.1.2. Raman spectra of MTA. The MTA powder was analyzed using Raman spectroscopy in the 50–3500 cm^{-1} region. The obtained spectrum in the region of 120–700 cm^{-1} is given in Fig. 2. The enlarged range from 450–700 cm^{-1} was also given in the inset. Bands in the region of 700–600 cm^{-1} can be assigned to Ti–O stretching vibrations, while in the region of 480–450 cm^{-1} can be assigned to stretching vibrations of Ti–O bonds with more considerable lengths than the Ti–O bonds which generate vibrational peaks in the area of 700–600 cm^{-1}.[27] In fact, the broadband at 640 cm^{-1} is split into a pair of bands with two slightly different intensities. The band in the region of 200–150 cm^{-1} can be assigned to O–Ti–O bending vibrations, confirming the presence of MTA.[27]

3.1.3. XRD analysis. The X-ray diffraction (XRD) patterns of Pulmoddai ilmenite raw material, commercially available bulk TiO_2 (anatase), and synthesized MTA are shown in Fig. 3. Intensive sharp peaks regarding the XRD pattern of Pulmoddai ilmenite can be reasonably assigned to the crystalline phase of $FeTiO_3$ in the raw material. Furthermore, anatase phase bulk TiO_2 revealed major XRD peaks at 2θ of 25.11°, 37.62°, 47.82°, 53.76°, 54.84° and 62.45°, from which peaks around 25° and 48° are well known to be most prominent over others and characteristic to the anatase TiO_2.[34,35]

The corresponding narrow and sharp diffraction peaks in the obtained XRD pattern can prove the crystalline nature of synthesized MTA. However, most importantly, hydrous titania ($TiO_2 \cdot H_2O$) in the anatase phase is erroneously described in literature as 'metatitanic acid' (H_2TiO_3) due to some structural similarities between the two compounds, thereby showing that 'metatitanic acid' exists as an amorphous compound owing to the presence of broader peaks at the same 2θ angles of the XRD spectrum of anatase phase crystalline TiO_2.[34,35] Conversely, it is clear that the obtained XRD pattern for synthesized MTA is entirely different compared to that of anatase TiO_2, where the characteristic peak of anatase TiO_2 at $2\theta = 47.82°$ is completely absent in the XRD pattern of synthesized MTA, although the reflection around $2\theta = 25°$ (25.11° for anatase TiO_2 and 24.54° for MTA) appears to be common for both the compounds. However, the presence of intensive sharp peaks such as $2\theta =$

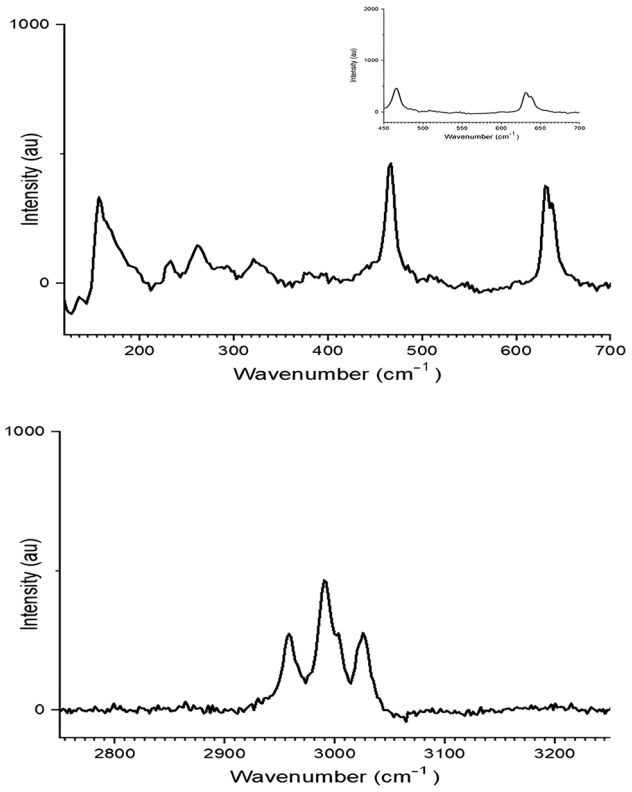

Fig. 2 Raman spectra of (a) Ti–O stretching and bending vibrations and (b) O–H stretching vibrations of MTA.

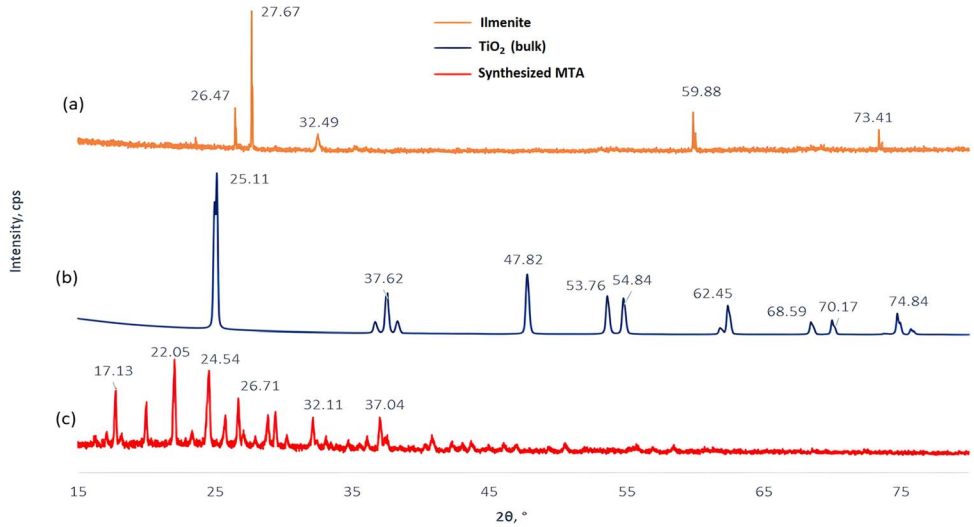

Fig. 3 X-Ray diffraction pattern of (a) ilmenite raw material (b) TiO_2 (bulk) and (c) synthesized MTA.

17.03°, 22.05°, and 26.71°, which were not observed for TiO_2, firmly verifies that H_2TiO_3 possesses a different crystalline structure compared to that of $TiO_2 \cdot H_2O$. In previously reported work, investigation of proton exchange with lithium titanate (Li_2TiO_3) to generate protonated form, H_2TiO_3, (MTA) possesses major reflections in the XRD pattern at $2\theta = 18.8°$ and 36.5°.[27] Therefore, sharp XRD peaks at $2\theta = 17.77°$ and 37.04° observed with our synthesized MTA can be sensibly attributed to the crystalline structure of MTA, which is different from anatase $TiO_2 \cdot H_2O$.

3.1.4. TGA analysis. The thermal stability of MTA was examined by thermo gravimetric analysis (TGA). The TGA of the synthesized MTA sample is shown in Fig. 4. The photocatalyst is described as an inner core with H_2TiO_3 molecules and outer shells composed of water molecules. The furthest shell is a shell chemisorbed monolayer of water. Therefore, the initial weight loss is observed due to the removal of hydrogen-bonded and non-hydrogen-bonded water molecules attached to the outer shell. This accounts for an approximate weight loss of 35% from the H_2TiO_3 sample. The subsequent gradual % weight loss of 34% occurred between 200 °C to 500 °C can be attributed to eliminating water molecules strongly bonded to acidic –OH groups of the H_2TiO_3 inner core. Beyond 538 °C, an approximate weight loss of 16% is credited to the calcination of H_2TiO_3 to TiO_2 in our developed process.

3.1.5. UV-visible spectrum of MTA. The UV-visible spectrum of MTA was obtained in the range of 200–800 nm, using deionized water as the blank solution, and it is shown in Fig. 5. The spectrum shows two prominent peaks in the UV region at 230 nm and 246 nm. Therefore, in this study, we could establish that these two peaks would be evident in having MTA.

3.1.6. SEM analysis of MTA. The SEM image of the synthesized MTA is depicted in Fig. 6. This image divulges that the particles are non-agglomerated, having cuboidal shapes with lengths on a micrometer scale.

3.2. Antibacterial assay

The inhibition zones observed in most of the LB plates inoculated with three bacterial species in separate plates revealed the antimicrobial activity of the three tested compounds: MTA, potassium titanate, and nano-titania (Fig. 7–9 and 12–14). The two disks, D and E, were loaded with 400 mg L^{-1} gentamicin

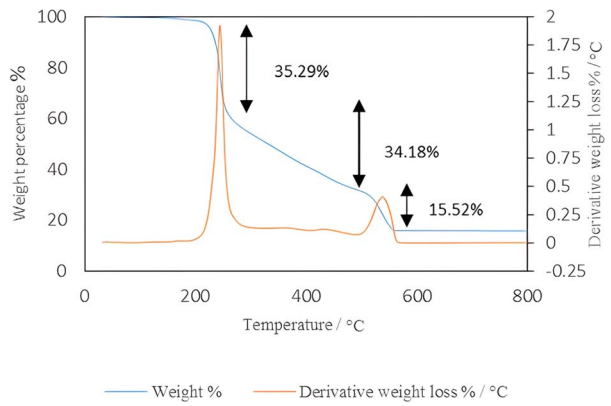

Fig. 4 Thermo gravimetric analysis of synthesized MTA.

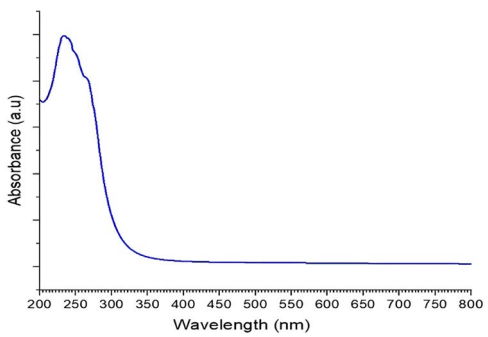

Fig. 5 UV-visible spectrum of synthesized MTA.

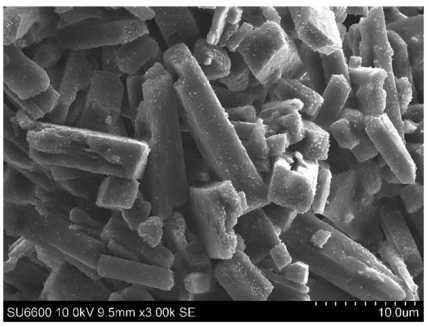

Fig. 6 SEM image of synthesized MTA.

(positive control) and sterile distilled water (negative control), respectively.

The mean inhibition zone diameters for different concentrations of MTA, potassium titanate, and nano-titania against those mentioned above three bacterial strains (*Pseudomonas* spp., *E. coli*, and *S. aureus*) were calculated and plotted as shown in Fig. 10 and 11.

According to the one-way ANOVA, the mean inhibition zone diameter significantly differed among the different concentrations of the MTA ($p < 0.05$) against *Pseudomonas* spp. at a 5% significant level in both dark and light conditions.

Under dark conditions, as shown in Fig. 7(a) and 10, standard antibiotic gentamicin against *Pseudomonas* spp. recorded the highest mean inhibition zone diameter of 17.5 ± 0.4 mm. The second (17.1 ± 0.7 mm), third (16.5 ± 0.4 mm), and fourth (16.3 ± 0.6 mm) highest mean inhibition zone diameters against *Pseudomonas* spp. were given by the MTA concentrations 400 mg L^{-1}, 500 mg L^{-1} and 450 mg L^{-1}, respectively, under dark conditions. According to the multiple mean comparison test, there were no significant differences with the mean inhibition zone diameter of gentamicin at 400 mg L^{-1}. These results indicated significantly high antibacterial activity of MTA at above three concentrations against the *Pseudomonas* spp. However, significantly lower mean inhibition zone diameters were given for the rest of the six concentrations, indicating low antibacterial activity at reduced concentrations. The improved antibacterial activity of the compound at higher

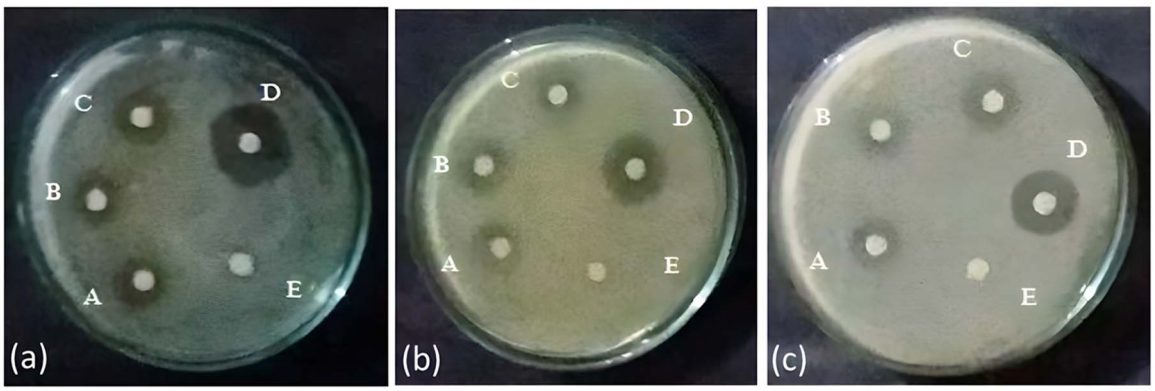

Fig. 7 (a) Inhibition zones given by MTA under dark conditions for the concentrations, (A) 400 mg L^{-1}, (B) 450 mg L^{-1}, (C) 500 mg L^{-1}, against *Pseudomonas* spp., (D) positive control (PC), (E) negative control (NC). (b) Inhibition zones given by MTA under dark conditions for the concentrations, (A) 400 mg L^{-1}, (B) 450 mg L^{-1}, (C) 500 mg L^{-1} against *E. coli*, (D) PC, (E) NC. (c) Inhibition zones given by MTA under dark conditions for the concentrations, (A) 250 mg L^{-1}, (B) 300 mg L^{-1}, (C) 350 mg L^{-1} against *S. aureus*, (D) PC, (E) NC.

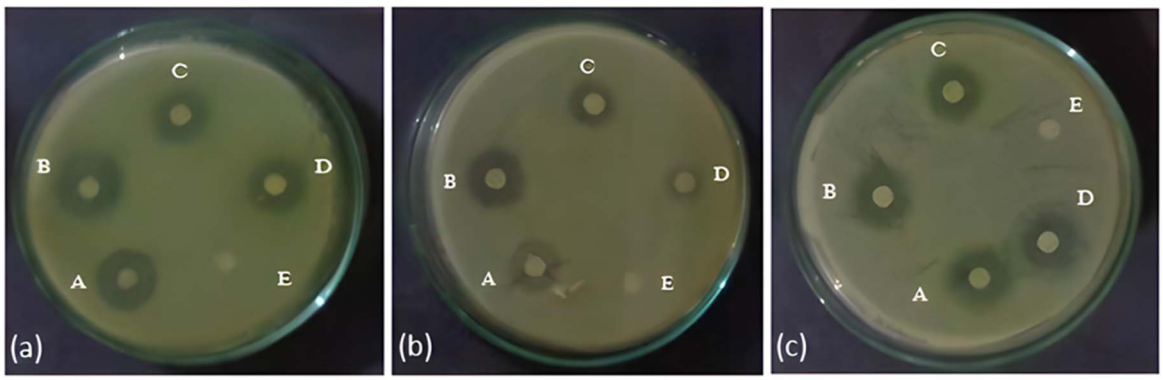

Fig. 8 (a) Inhibition zones given by potassium titanate under dark conditions for the concentrations, (A) 400 mg L^{-1}, (B) 450 mg L^{-1}, (C) 500 mg L^{-1} against *Pseudomonas* spp., (D) PC, (E) NC. (b) Inhibition zones given by potassium titanate under dark conditions for the concentrations, (A) 400 mg L^{-1}, (B) 450 mg L^{-1}, (C) 500 mg L^{-1} against *E. coli*, (D) PC, (E) NC. (c) Inhibition zones given by potassium titanate under dark conditions for the concentrations, (A) 400 mg L^{-1}, (B) 450 mg L^{-1}, (C) 500 mg L^{-1} against *S. aureus*, (D) PC, (E) NC.

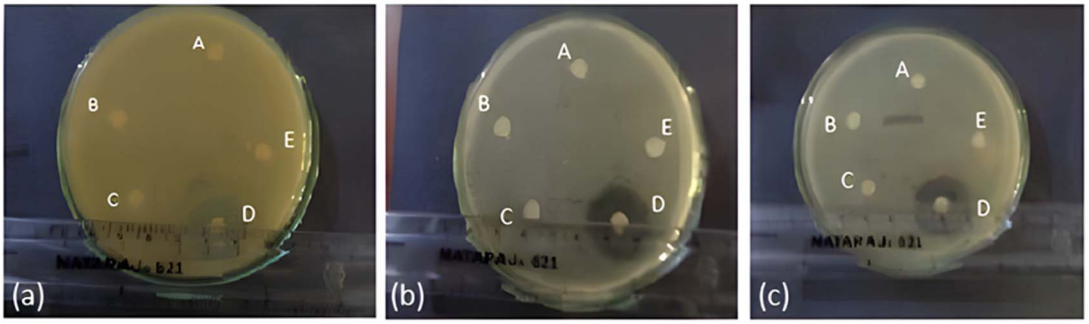

Fig. 9 (a) Inhibition zones given by nano-titania under dark conditions for the concentrations, (A) 400 mg L^{-1}, (B) 450 mg L^{-1}, (C) 500 mg L^{-1} against *Pseudomonas* spp., (D) PC, (E) NC. (b) Inhibition zones given by nano-titania under dark conditions for the concentrations, (A) 400 mg L^{-1}, (B) 450 mg L^{-1}, (C) 500 mg L^{-1} against *E. coli*, (D) PC, (E) NC. (c) Inhibition zones given by nano-titania under dark conditions for the concentrations, (A) 400 mg L^{-1}, (B) 450 mg L^{-1}, (C) 500 mg L^{-1} against *S. aureus* (D) PC, (E) NC.

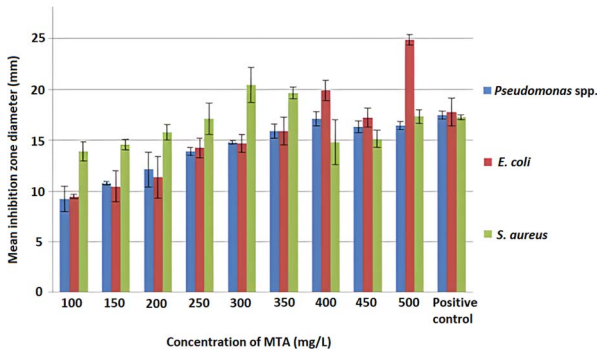

Fig. 10 Mean inhibition zone diameter shown by different concentrations of MTA against *Pseudomonas* spp., *E. coli* and *S. aureus*, under dark conditions.

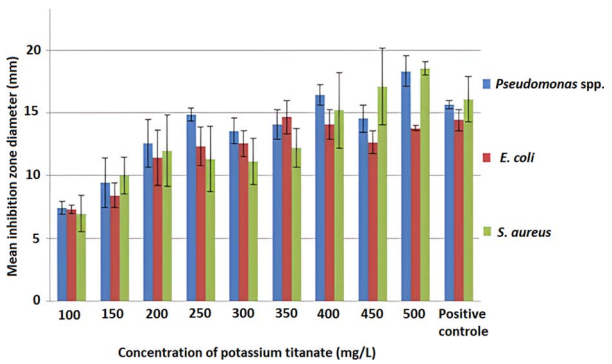

Fig. 11 Mean inhibition zone diameters shown by different concentrations of potassium titanate against *Pseudomonas* spp., *E. coli* and *S. aureus*, under dark conditions.

concentrations could be accredited to the enhanced interaction between MTA and the bacteria, where the optimum MTA concentration was found to be 400 mg L^{-1}. However, the weakening of the antibacterial activity with higher MTA concentrations of 450 mg L^{-1} and 500 mg L^{-1} can be attributed to unexpected effects such as saturation or precipitation of the compound under these exceedingly high concentrations, as MTA is prone to get precipitated, causing lower interactions with the bacteria.

However, as shown in Fig. 12(a), the presence of light has further improved the antibacterial activity of MTA against *Pseudomonas* spp. The highest mean inhibition diameter (20.2 $\pm$ 0.4 mm) resulted from the MTA concentration of 400 mg L^{-1}, exhibiting its superiority even compared to gentamicin (17.9 $\pm$ 0.7) under light exposure.

Compared to *Pseudomonas* spp., MTA showed elevated antibacterial activity against *E. coli*. In terms of both light-dependent and light-independent activity, the mean inhibition zone diameter demonstrated for *E. coli* significantly differed among the different concentrations ($p < 0.05$) of MTA at a 5% significant level.

Under dark conditions, the highest mean inhibition zone diameter of 24.9 $\pm$ 0.5 mm was observed for *E. coli* in 500 mg L^{-1} of MTA (Fig. 7(b) and 10). The second highest mean inhibition zone diameter of 19.9 $\pm$ 1.0 mm was shown by the concentration of 400 mg L^{-1} of MTA. These two concentrations resulted in significantly higher mean inhibition zone diameters for *E. coli*, where the effect of MTA was greater than that of gentamicin, even in the absence of light. There was no significant difference between MTA and gentamicin for mean inhibition zone diameters recorded at 450 mg L^{-1} and 350 mg L^{-1} of MTA. Lower concentrations of MTA (100–300 mg L^{-1}) had shown significantly lower mean inhibition zone diameters than gentamicin. The effectiveness of MTA in inhibiting the growth of *E. coli* under dark conditions was clearly evident by the experiment's results. Fig. 10 reveals that, compared to the *Pseudomonas* spp., *E. coli* was more susceptible to the light-independent antibacterial activity of MTA at the concentrations of 500 mg L^{-1} and 400 mg L^{-1}.

However, the irradiation of light further increased the antibacterial action of MTA, compared to dark conditions, resulting in higher inhibition zone diameters against *E. coli* (Fig. 12(b)). Likewise, the mean inhibition zone at the MTA concentration of 500 mg L^{-1} could be expanded from the diameter of 24.9 $\pm$

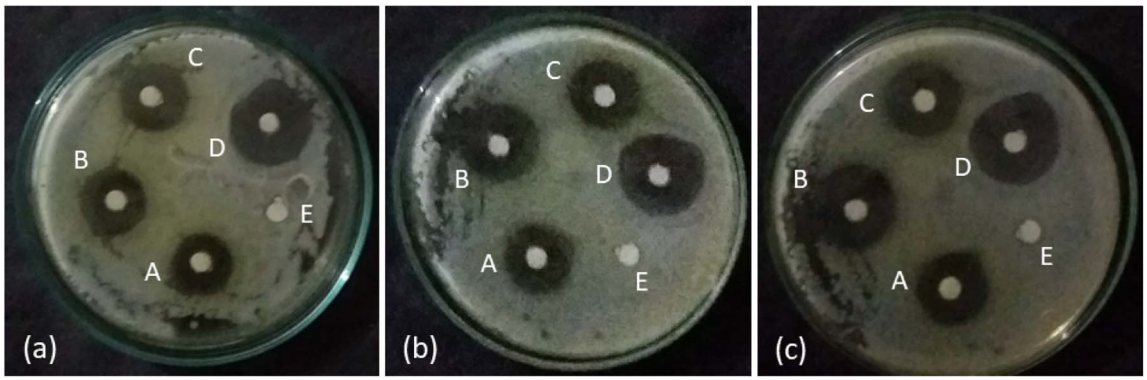

Fig. 12 (a) Inhibition zones given by MTA under light irradiation for the concentrations, (A) 400 mg L^{-1}, (B) 450 mg L^{-1}, (C) 500 mg L^{-1}, against *Pseudomonas* spp., (D) positive control (PC), (E) negative control (NC). (b) Inhibition zones given by MTA under light irradiation for the concentrations, (A) 400 mg L^{-1}, (B) 450 mg L^{-1}, (C) 500 mg L^{-1} against *E. coli*, (D) PC, (E) NC. (c) Inhibition zones given by MTA under light irradiation for the concentrations, (A) 250 mg L^{-1}, (B) 300 mg L^{-1}, (C) 350 mg L^{-1} against *S. aureus*, (D) PC, (E) NC.

0.5 mm up to 25.5 ± 0.2 mm in the presence of light. Similarly, the mean inhibition zone diameter could be widened from 19.9 ± 1.0 mm up to 21.4 ± 0.9 mm with light assistance for the 400 mg L^{-1} MTA concentration. These results further conclude that the photon energy can enhance the antibacterial capability of MTA.

Concerning *S. aureus*, the inhibitory effect was significantly different among the different concentrations of MTA ($p < 0.05$) at a 5% significant level. According to Fig. 7(c) and 10, the highest activities in the dark condition, as reflected by mean inhibition zone diameters (20.4 ± 1.7 mm and 19.7 ± 0.6 mm), were recorded at concentrations of 300 mg L^{-1} and 350 mg L^{-1} of MTA, respectively, which is also higher than the activity of gentamicin (17.3 ± 0.3 mm). The remaining concentrations showed growth inhibition (500 mg L^{-1}, 250 mg L^{-1}, and 200 mg L^{-1}), which was not as high as gentamicin. Among the tested nine concentrations, five showed intense antibacterial activity against *S. aureus*, confirming the effectiveness of the MTA as an antibacterial compound. As observed with the two above bacterial species, the antibacterial action of MTA under the influence of light was higher for *S. aureus* as well (Fig. 12(c)). Mean inhibition zone diameters were 22.6 ± 0.2 mm and 21.9 ± 0.7 mm for 300 mg L^{-1} and 350 mg L^{-1} respectively. In outline, MTA against three bacterial strains tested under dark conditions revealed that the Gram-positive bacteria were more affected by the MTA, and it is a more powerful antibacterial compound than the standard gentamicin, even under dark conditions. Optimized MTA concentrations can be listed as 500 mg L^{-1}, 400 mg L^{-1}, and 300 mg L^{-1} for *E. coli*, *Pseudomonas* spp., and *S. aureus* respectively. However, optimum MTA concentration was found to vary depending upon the bacterial species, and this variation could be reasonably ascribed to the membrane permeability, resistance mechanisms, genetic makeup, and different metabolic pathways of the bacteria, resulting in disparities in the susceptibility to external compounds.[2–4]

Fig. 8(a) and 11 reveal results that we obtained with potassium titanate against *Pseudomonas* spp. Accordingly, potassium titanate could be recognized as a more potent antibacterial agent in dark and light conditions. The mean inhibition zone diameters significantly differed among the different concentrations of potassium titanate ($p < 0.05$) at a 5% significant level. The highest mean inhibition zone diameter of 18.3 ± 1.2 mm was observed in the 500 mg L^{-1} concentration of potassium titanate, and it was significantly higher than that of the 400 mg L^{-1} concentration of gentamicin. The 400 mg L^{-1} gave the second-highest mean inhibition zone (16.4 ± 0.8 mm), and it was not significantly higher than the third-highest mean inhibition zone (15.7 ± 0.3 mm) given by gentamicin. Potassium titanate concentrations of 250 mg L^{-1} and 450 mg L^{-1} also recorded mean inhibition zone diameters, which were not significantly different from those of gentamicin. Four concentrations of potassium titanate (300 mg L^{-1}, 200 mg L^{-1}, 150 mg L^{-1}, and 100 mg L^{-1}) showed significantly lower mean inhibition zone diameters against *Pseudomonas* spp. enhanced antibacterial activity of potassium titanate against *Pseudomonas* spp. was observed for all nine concentrations under the influence of light (Fig. 13(a)). The maximum light-dependent action against *Pseudomonas* spp. was also revealed for the potassium titanate concentration of 500 mg L^{-1}, resulting in a mean inhibition diameter of 20.1 ± 0.7 mm. Overall results concluded the suitability of potassium titanate for the control of growth of *Pseudomonas* spp. due to the markedly higher activities recorded.

Overall, both light-dependent and light-independent antibacterial activity of potassium titanate recorded against *E. coli* was at lower levels than that of *Pseudomonas* spp. The mean inhibition zone diameter measured against *E. coli* for different compound concentrations was significantly different at a 5% significant level ($p < 0.05$).

Following Fig. 8(b) and 11, the 350 mg L^{-1} of potassium titanate recorded the highest mean inhibition zone diameter of 14.7 ± 1.3 mm, under dark conditions and was not significantly higher than the inhibition zones recorded by 400 mg L^{-1} of gentamicin. Concentrations of 400 mg L^{-1}, 500 mg L^{-1} and 450 mg L^{-1} of potassium titanate recorded inhibition zone diameters of 14.1 ± 0.8 mm, 13.8 ± 0.2 mm and 12.7 ± 0.9 mm,

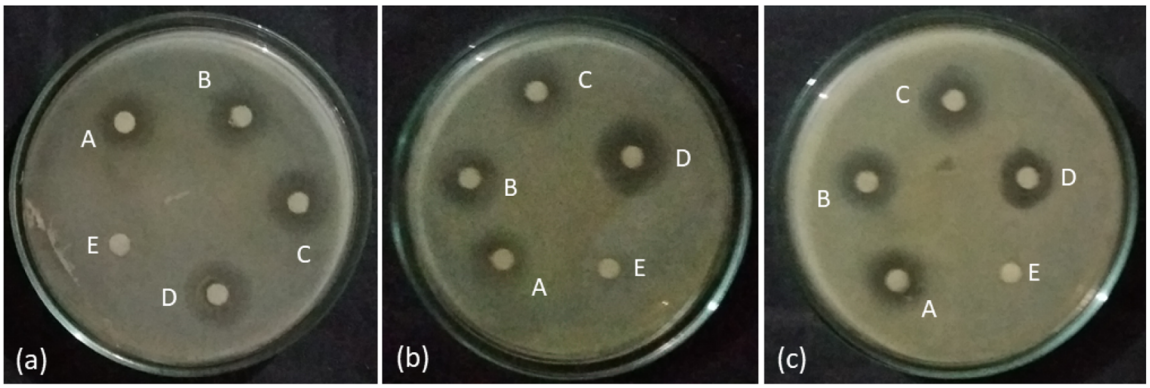

Fig. 13 (a) Inhibition zones given by potassium titanate under light irradiation for the concentrations, (A) 400 mg L^{-1}, (B) 450 mg L^{-1}, (C) 500 mg L^{-1} against *Pseudomonas* spp., (D) PC, (E) NC. (b) Inhibition zones given by potassium titanate under light irradiation for the concentrations, (A) 400 mg L^{-1}, (B) 450 mg L^{-1}, (C) 500 mg L^{-1} against *E. coli*, (D) PC, (E) NC. (c) Inhibition zones given by potassium titanate under light irradiation for the concentrations, (A) 400 mg L^{-1}, (B) 450 mg L^{-1}, (C) 500 mg L^{-1} against *S. aureus*, (D) PC, (E) NC.

respectively. However, among the tested nine concentrations of potassium titanate, five concentrations gave a non-significant reaction to that of gentamicin. These results also indicated the effective antibacterial activity of potassium titanate against *E. coli*, even without photon energy, exerting a similar effect as the standard antibiotic gentamicin. However, under the influence of light, a greater mean inhibition zone diameter (16.2 ± 0.9 mm) was recorded for potassium titanate in the concentration of 350 mg L^{-1}, compared to gentamicin (14 ± 0.4 mm) against *E. coli*.

Moreover, comparatively higher antibacterial activity of potassium titanate against *S. aureus* was observed than other two species with significantly different ($p < 0.05$) mean inhibition zones at a 5% significant level. Fig. 8(c) and 11 disclose that the highest inhibition zone diameter of 18.6 ± 0.5 mm was recorded by the potassium titanate concentration of 500 mg L^{-1} followed by 450 mg L^{-1} (17.1 ± 0.3 mm), under dark conditions. These two values were not notably higher than the third-highest mean inhibition zone diameter of 16.1 ± 1.8 mm recorded by gentamicin. Six concentrations of potassium titanate recorded significantly lower mean inhibition zone diameters against *S. aureus* than gentamicin, showing reduced antibacterial activity at lower concentrations.

The light-dependent activity of potassium titanate was only slightly elevated against *S. aureus*, where the highest inhibition zone diameter (19.2 ± 0.8 mm) was recorded for the concentration of 500 mg L^{-1} (Fig. 13(c)).

When the light-independent antibacterial activity of potassium titanate was compared against three bacteria, potassium titanate is a more potent antibacterial compound against *Pseudomonas* spp. and *S. aureus* than *E. coli*. Potassium titanate concentrations can be optimized as 500 mg L^{-1} for both *Pseudomonas* spp. and *S. aureus*, whereas 350 mg L^{-1} for *E. coli*, under dark conditions. Further, several concentrations of potassium titanate exhibited high antibacterial activity compared to gentamicin at 400 mg L^{-1}.

The third compound, nano-titania did not show antibacterial activity at all nine concentrations against *E. coli*, *S. aureus*, and *Pseudomonas* spp. (Fig. 9(a–c)) under the dark conditions used in the experiment. However, as revealed in Fig. 14(a–c), nano-titania was successful against the three bacterial strains only in the presence of light, where the mean inhibition zone diameter, recorded for the bacterial species in the presence of different concentrations of nano-titania, was significantly different at a 5% significant level ($p < 0.05$). The highest inhibition zone diameters of 14.9 ± 0.4 mm, 14.3 ± 0.9 mm, and 12.7 ± 0.7 mm were obtained for *Pseudomonas* spp., *S. aureus*, and *E. coli*, respectively, at the nano-titania concentration of 400 mg L^{-1}.

Fig. 15 depicts the comparison of the susceptibility of the three bacterial strains, *i.e.*, *Pseudomonas* spp., *E. coli*, and *S. aureus*, towards the optimized concentrations of MTA, potassium titanate, and nano-titania, under both dark and light conditions. Both *Pseudomonas* spp. and *S. aureus* possess a greater vulnerability towards MTA and potassium titanate than nano-titania in the presence and absence of light. However, *E. coli* was more affected by MTA than potassium titanate in dark and light conditions. In accordance with the measured inhibition zone diameters, it is clear that the light-independent antibacterial activity of both MTA and potassium titanate was even greater than the light-dependent antibacterial activity of nano-titania. Since the light-independent activity becomes significant in clinical applications, it was evident that MTA and potassium titanate gain merits over nano-titania as effective antibacterial agents. The light-dependent antibacterial activity of nano-titania and the enhanced activity of MTA and potassium titanate under light exposure can be reasonably assigned to the photocatalytic damage to the bacteria caused by Reactive Oxygen Species (ROS), which can be produced by these three compounds in the presence of photon energy.[36–44] Most significantly, the light-independent antibacterial activity of MTA and potassium titanate should be explained without regard to the photocatalytic effect due to the absence of photon energy. Although MTA and potassium titanate have not been explored in antimicrobial applications under dark conditions by previous studies, the mechanism of light-independent action

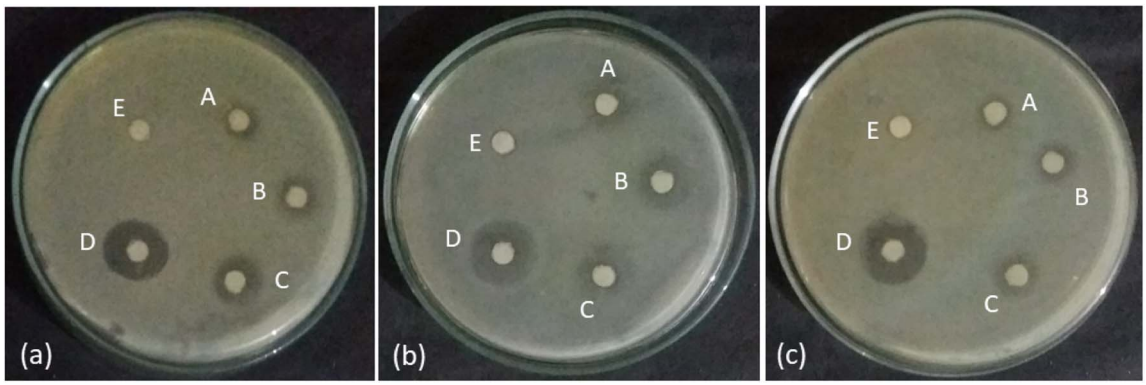

Fig. 14 (a) Inhibition zones given by nano-titania under light irradiation for the concentrations, (A) 400 mg L^{-1}, (B) 450 mg L^{-1}, (C) 500 mg L^{-1} against *Pseudomonas* spp., (D) PC, (E) NC. (b) Inhibition zones given by nano-titania under light irradiation for the concentrations, (A) 400 mg L^{-1}, (B) 450 mg L^{-1}, (C) 500 mg L^{-1} against *E. coli*, (D) PC, (E) NC. (c) Inhibition zones given by nano-titania under light irradiation for the concentrations, (A) 400 mg L^{-1}, (B) 450 mg L^{-1}, (C) 500 mg L^{-1} against *S. aureus* (D) PC, (E) NC.

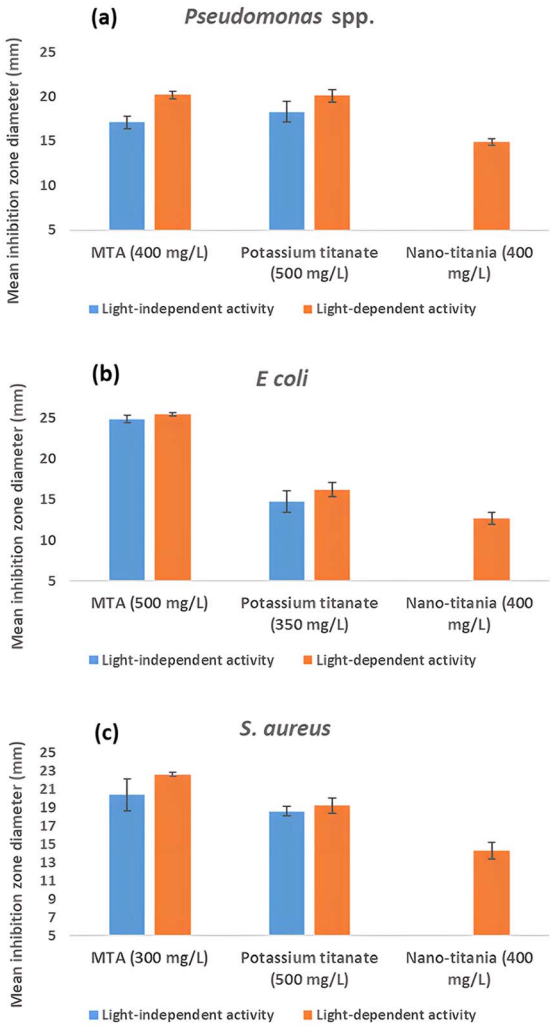

Fig. 15 Comparison of the mean inhibition zone diameters measured against (a) *Pseudomonas* spp. (b) *E. coli* and (c) *S. aureus*, at the optimized concentrations of MTA, potassium titanate and nano-titania, in terms of their light-independent and light-dependent antibacterial activities.

of the two species against bacteria can be assessed under similar compounds reported in the literature.[45–50] The electron-capturing ability of the Schottky junction created between Fe and titanium oxide has been attributed to the cause of oxidation damage to *S. aureus* under dark conditions.[45] A similar study reports the light-independent antibacterial action of ZnO nanoparticles against *S. aureus* and *Klebsiella pneumoniae*, as its attachment to bacterial cell wall. The impact of ZnO on the bacteria is related to the local dissolution of adsorbed ZnO and thus elevated Zn^{2+} concentration in the bacterial cytoplasm.[46] Light-independent antimicrobial activity of ZnO against *E. coli* has also been related to ROS generated from the surface of the compound[47] as well as defects on ZnO surface.[50] The significance of possessing surface defects on antimicrobial compounds has been further verified through the contact-based antimicrobial action of MgO against *E. coli*, *S. epidermidis* and *Pseudomonas* spp.[49]

In our study, both MTA and potassium titanate were successful towards both Gram-positive and Gram-negative bacterial strains, implying several possible pathways for their mechanism of action in the absence of light. Therefore, the light-independent mechanism can be predicted as follows (Fig. 16).

The light-independent mechanism of action can be mainly supposed to be through the interaction of the antipathogenic material with the bacterial cell wall, eventually exerting harmful effects on the microbe due to the membrane's disintegration and the cytoplasmic material's leakage. Adsorption of bacteria on the antimicrobial material is expected to improve the extent of interactions with the cell wall and, therefore, alters the cell membrane integrity even without photon energy.[27,46,48] Moreover, being titanium-based catalytic materials, the bactericidal potential of MTA and potassium titanate can be related to their super-hydrophilic properties as well as to their defect sites, which is predicted to possess a greater oxidation tendency due to the presence of oxygen vacancies and Ti^{4+} in higher concentrations. The presence of such defects causes the generation of ROS upon contact with O_2, and ROS generated can profoundly have a detrimental impact on pathogens.[47–50]

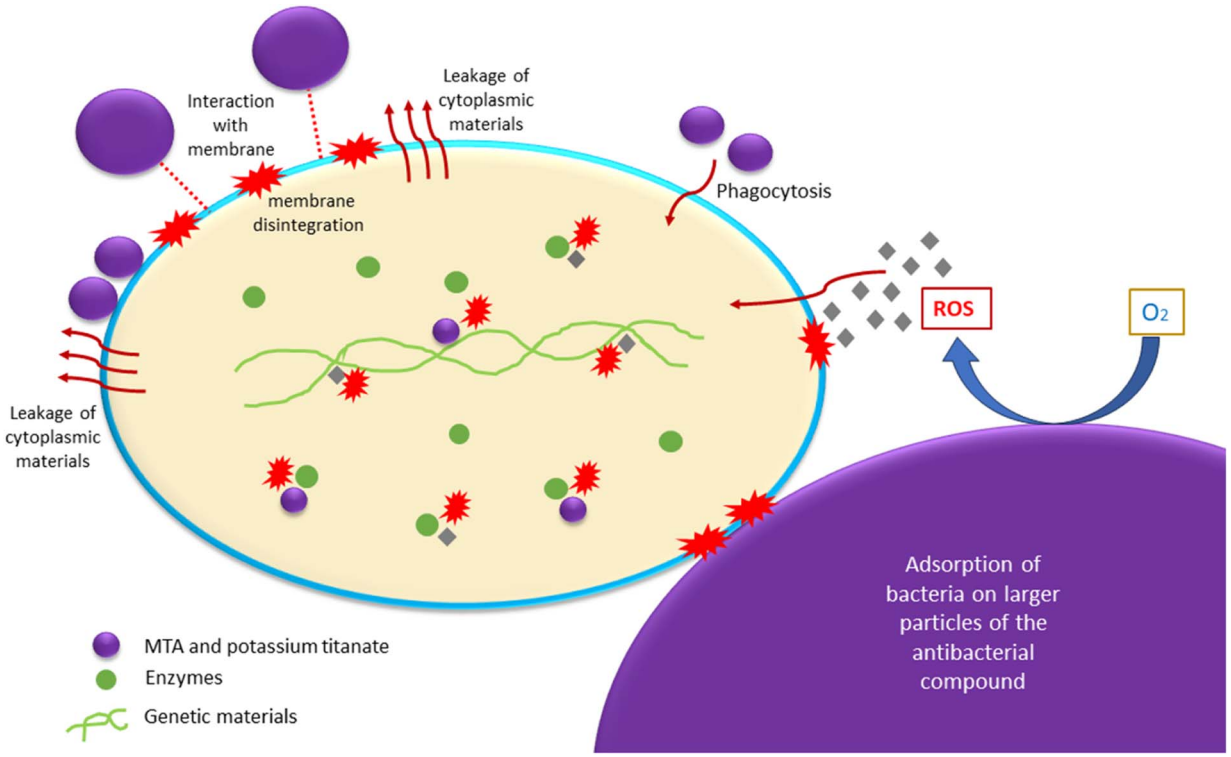

Fig. 16 Proposed mechanisms for the light-independent antibacterial action of MTA and potassium titanate.

Furthermore, it can be suggested that the direct contact of MTA and potassium titanate with bacterial cell walls leads to phagocytosis of the titanium species by microbes, resulting in alterations of the cytoplasm composition and thereby, hindering vital biochemical processes of the cell.[48,51]

4 Conclusions

The stable intermediates, MTA and potassium titanate, which were isolated from our novel process, successfully exhibited light-dependent and light-independent antibacterial properties against *Pseudomonas* spp., *E. coli*, and *S. aureus*.

MTA exhibited light-independent antibacterial properties against all three bacterial species at 100–500 mg L^{-1} concentrations. For *E. coli*, 400 mg L^{-1} and 500 mg L^{-1} concentrations showed superior antibacterial properties compared to the positive control, gentamicin. For *S. aureus*, the light-independent effect of 300 mg L^{-1} and 350 mg L^{-1} MTA concentrations was also more significant than gentamicin. For *Pseudomonas* spp. under dark conditions, optimum MTA concentrations of 400–500 mg L^{-1} were more effective; however, the effect was comparatively lower than that of gentamicin.

Greater antibacterial activity of potassium titanate was found against the three bacterial species. Significantly, the antibacterial activity of potassium titanate (500 mg L^{-1}) under dark conditions was superior against *Pseudomonas* spp. over the positive control. The concentration of potassium titanate could be optimized as 350 mg L^{-1} and 500 mg L^{-1} for *E. coli* and *S. aureus*, respectively; however, the light-independent antibacterial effect of the compound was not more significant than that of gentamicin. A well-known antibacterial agent, nano-titania, completely failed to inhibit the growth of any of the bacteria tested under dark conditions. The antibacterial activity of all three titanium compounds, *i.e.*, MTA, potassium titanate, and nano-titania, was enhanced under the influence of light against all three bacterial species. This study identified the light-independent antibacterial effect of MTA and potassium titanate as superior to the light-dependent effect of nano-titania. Another important point is that both MTA and potassium titanate are effective against Gram-positive and Gram-negative bacterial strains, *i.e.*, showing a broad spectrum of activity in both dark and light conditions, an uncommon phenomenon concerning antibacterial compounds. Hence, these two compounds will have a definite advantage over common antibiotics in clinical applications.

Author contributions

N. D. Wickramasinghe: methodology, formal analysis, data curation, writing-original draft; A. H. J. Sampath: writing-original draft, writing-review, and editing, formal analysis, visualization; C. M. Nanayakkara: supervision (anti-microbial work), resources, writing-review and editing; K. M. Nalin de Silva: supervision, resources, writing-review, and editing; Rohini M. de Silva: conceptualization, supervision, resources, writing-review and editing. All the authors have read and agreed to the published version of the manuscript.

Conflicts of interest

The authors declare no conflict of interest.

References

1 E. R. Sydnor and T. M. Perl, *Clin. Microbiol. Rev.*, 2011, **24**, 141–173.
2 K. Ulanowska, A. Tkaczyk, G. Konopa and G. Węgrzyn, *Arch. Microbiol.*, 2005, **184**, 271–278.
3 A. Tanitame, Y. Oyamada, K. Ofuji, M. Fujimoto, N. Iwai, Y. Hiyama, K. Suzuki, H. Ito, H. Terauchi, M. Kawasaki, K. Nagai, M. Wachi and J.-i. Yamagishi, *J. Med. Chem.*, 2004, **47**, 3693–3696.
4 A. Rodríguez-Rojas, J. Rodríguez-Beltrán, A. Couce and J. Blázquez, *Int. J. Med. Microbiol.*, 2013, **303**, 293–297.
5 M. Montazer, A. Behzadnia, E. Pakdel, M. K. Rahimi and M. B. Moghadam, *J. Photochem. Photobiol., B*, 2011, **103**, 207–214.
6 H. A. Foster, I. B. Ditta, S. Varghese and A. Steele, *Appl. Microbiol. Biotechnol.*, 2011, **90**, 1847–1868.
7 Q. Li, S. Mahendra, D. Y. Lyon, L. Brunet, M. V. Liga, D. Li and P. J. J. Alvarez, *Water Res.*, 2008, **42**, 4591–4602.
8 Y. H. Tsuang, J. S. Sun, Y. C. Huang, C. H. Lu, W. H. S. Chang and C. C. Wang, *Artif. Organs*, 2008, **32**, 167–174.
9 Y. Xie, Y. He, P. L. Irwin, T. Jin and X. Shi, *Appl. Environ. Microbiol.*, 2011, **77**, 2325–2331.
10 T. Jin, D. Sun, J. Y. Su, H. Zhang and H. J. Sue, *J. Food Sci.*, 2009, **74**, M46–M52.
11 P. J. Espitia, N. de. Soares, J. S. Coimbra, N. J. de Andrade, R. S. Cruz and E. A. Medeiros, *Food Bioprocess Technol.*, 2012, **5**, 1447–1464.
12 J. Sawai, *J. Microbiol. Methods*, 2003, **54**, 177–182.
13 K. R. Raghupathi, R. T. Koodali and A. C. Manna, *Langmuir*, 2011, **27**, 4020–4028.
14 A. Azam, *Int. J. Nanomed.*, 2012, **7**, 3527–3535.
15 M. Černík and V. V. T. Padil, *Int. J. Nanomed.*, 2013, **8**, 889–898.
16 S. Jadhav, S. Gaikwad, M. Nimse and A. Rajbhoj, *J. Cluster Sci.*, 2011, **22**, 121–129.
17 I. Sondi and B. Salopek-Sondi, *J. Colloid Interface Sci.*, 2004, **275**, 177–182.
18 M. Rai, A. Yadav and A. Gade, *Biotechnol. Adv.*, 2009, **2**, 76–83.
19 V. K. Sharma, R. A. Yngard and Y. Lin, *Adv. Colloid Interface Sci.*, 2009, **145**, 83–96.
20 A. J. Huh and Y. J. Kwon, *J. Controlled Release*, 2011, **156**, 128–145.
21 C. You, C. Han, X. Wang, Y. Zheng, Q. Li, X. Hu and H. Sun, *Mol. Biol. Rep.*, 2012, **39**, 9193–9201.
22 Z. X. Lu, L. Zhou, Z. L. Zhang, W. L. Shi, Z. X. Xie, H. Y. Xie, D. W. Pang and P. Shen, *Langmuir*, 2003, **19**, 8765–8768.
23 T. Paul, P. L. Miller and T. J. Strathmann, *Environ. Sci. Technol.*, 2007, **41**, 4720–4727.
24 G. Fu, P. S. Vary and C. T. Lin, *J. Phys. Chem. B*, 2005, **109**, 8889–8898.
25 D. K. Lee, D. W. Kim, I. S. Cho, S. Lee, J. Noh and K. S. Hong, *J. Nanosci. Nanotechnol.*, 2010, **10**, 1361–1366.
26 N. Wang, D. Kong and H. He, *Powder Technol.*, 2011, **207**, 470–473.
27 T. A. Denisova, L. G. Maksimova, E. V. Polyakov, N. A. Zhuravlev, S. A. Kovyazina, O. N. Leonidova, D. F. Khabibulin and E. I. Yur'eva, *Russ. J. Inorg. Chem.*, 2006, **51**, 691–699.
28 Y. V. Baklanova, L. G. Maksimova, N. A. Zhuravlev, V. Y. Kavun and T. A. Denisova, *Bull. Russ. Acad. Sci.: Phys.*, 2010, **74**, 1097–1099.
29 H. Fujikawa and K. Tanabe, *US Pat.*, 5935608A, 1999.
30 A. M. Olsson and L. Salmén, *Carbohydr. Res.*, 2004, **339**, 813–818.
31 L. M. Kustov, V. Y. Borovkov and V. B. Kazansky, *J. Catal.*, 1981, **72**, 149–159.
32 F. Haase and J. Sauer, *J. Am. Chem. Soc.*, 1998, **120**, 13503–13512.
33 B. C. Viana, O. P. Ferreira, A. G. Filho, A. A. Hidalgo, J. M. Filho and O. L. Alves, *Vib. Spectrosc.*, 2011, **55**, 183–187.
34 C. Tian, *Mater. Chem. Phys.*, 2019, **232**, 409–413.
35 Z. Wang, K. Chen, J. Zhu, X. Zhou and F. Lin, *IOP Conf. Ser.: Mater. Sci. Eng.*, 2019, **562**, 1–9.
36 K. S. Khashan, G. M. Sulaiman, F. A. Abdulameer, S. Albukhaty, M. A. Ibrahem, T. Al-Muhimeed and A. A. AlObaid, *Appl. Sci.*, 2021, **11**, 4623.
37 K. P. Priyanka, T. H. Sukirtha, K. M. Balakrishna and T. Varghese, *IET Nanobiotechnol.*, 2016, **10**, 81–86.
38 X. Yu, H. Chen, Q. Ji, Y. Chen, Y. Wei, N. Zhao and B. Yao, *Chemosphere*, 2021, **267**, 129285.
39 X. Yu, J. Zhang, J. Zhang, J. Niu, J. Zhao, Y. Wei and B. Yao, *Chem. Eng. J.*, 2019, **374**, 316–327.
40 J. Nie, X. Yu, Z. Liu, J. Zhang, Y. Ma, Y. Chen, Q. Ji, N. Zhao and Z. Chang, *J. Clean. Prod.*, 2022, **363**, 132593.
41 X. Yu, J. Zhang, Y. Chen, Q. Ji, Y. Wei, J. Niu, Z. You and B. Yao, *J. Environ. Chem. Eng.*, 2021, **9**, 106161.
42 J. Nie, X. Yu, Z. Liu, Y. Wei, J. Zhang, N. Zhao, Z. Yu and B. Yao, *Appl. Surf. Sci.*, 2022, **576**, 151842.
43 J. Nie, X. Yu, Y. Wei, Z. Liu, J. Zhang, Z. Yu, Y. Ma and B. Yao, *Process Saf. Environ. Prot.*, 2023, **170**, 241–258.
44 F. Yang, X. Yu, K. Wang, Z. Liu, Z. Gao, T. Zhang, J. Niu, J. Zhao and B. Yao, *J. Alloys Compd.*, 2023, **960**, 170716.
45 Y. Tian, H. Cao, Y. Qiao, F. Meng and X. Liu, *Acta Biomater.*, 2014, **10**, 4505–4517.
46 A. Joe, S. H. Park, K. D. Shim, D. J. Kim, K. H. Jhee, H. W. Lee, C. H. Heo, H. M. Kim and E. S. Jang, *J. Ind. Eng. Chem.*, 2017, **25**, 430–439.
47 K. Hirota, M. Sugimoto, M. Kato, K. Tsukagoshi, T. Tanigawa and H. Sugimoto, *Ceram. Int.*, 2010, **36**, 497–506.
48 C. Thambiliyagodage, L. Usgodaarachchi, M. Jayanetti, C. Liyanaarachchi, M. Kandanapitiye and S. Vigneswaran, *ACS Omega*, 2022, **7**, 25403–25421.
49 N. Anicic, M. Vukomanovic, T. Koklic and D. Suvorov, *Small*, 2018, **14**(26), 1800205.
50 V. L. Prasanna and R. Vijayaraghavan, *Langmuir*, 2015, **31**, 9155–9162.
51 C. Rosales and E. Uribe-Querol, *BioMed Res. Int.*, 2017, 9042851.